# Optimal Descending, Hypersonic Turn to Heading

G. Richard Eisler*
*Sandia National Laboratories, Albuquerque, New Mexico*
and
David G. Hull†
*University of Texas at Austin, Austin, Texas*

**Approximate optimal controls are formulated for a re-entry vehicle to execute a maximum-terminal-velocity turn to a specified heading while executing a steep descent trajectory. A Newton scheme is used to repetitively solve a nonlinear algebraic system for two parameters in the control equations to provide the on-line guidance. Trajectory comparisons from a continuous solution of the optimal control problem, pure numerical optimization, and simulation of sample-data guidance show good agreement, if the atmospheric model is accurate.**

## Nomenclature

| | |
|---|---|
| $A$ | $=(\tau^3+d\tau^2+e\tau+f)^{1/2}$ |
| $a,b,c$ | =cubic roots of $A=0$ |
| $C_D,C_L,C_S$ | =drag, lift, and side force coefficients |
| $C_{D_0}$ | =zero-lift drag coefficient |
| $C_L^*$ | =lift coefficient at max $L/D$ |
| $d,e,f$ | =coefficients in cubic radical in Eq. (34) |
| $D,L,S$ | =drag, lift, and side forces, lb |
| $F,E,\Pi$ | =elliptic integrals of the first, second, and third kinds |
| $g$ | =gravitational acceleration, ft/s$^2$ |
| $G,H$ | =end function and Hamiltonian |
| $h$ | =altitude above mean sea level, ft |
| $j,k,l,m$ | =elliptic integral moduli |
| $m$ | =mass, slugs |
| $M,\bar{M}$ | =Loh's constant forms |
| $n$ | $=2/\sqrt{a-c}$ |
| $p_u,p_w,p_\chi$ | =Lagrange multipliers for state equations |
| $r$ | =distance from center of Earth, ft |
| $S_R$ | =vehicle reference area, ft |
| $t$ | =time, s |
| $u$ | =negative logarithm of velocity |
| $v$ | =generic function in Eq. (34) |
| $V$ | =velocity, ft/s |
| $w$ | =dimensionless density |
| $X_\pm$ | =combined elliptic integral forms for $\chi$ |
| $x$ | =generic variable in Eq. (34) |
| $xyz$ | =local-horizon coordinate directions |
| $XYZ$ | =Earth-centered inertial coordinate directions |
| $\beta_a$ | =atmospheric scale height, ft |
| $\gamma,\chi$ | =flight-path and heading angles, deg |
| $\delta,\Delta,\mu,\omega$ | =elliptic integral arguments |
| $\theta,\phi$ | =inertial longitude and latitude angles |
| $\kappa$ | =fit constant in parabolic drag polar |
| $\lambda,\sigma$ | =normalized lift and side force coefficients |
| $\nu$ | =Lagrange multipliers for end constraints |
| $\rho$ | =atmospheric density, slugs/ft$^3$ |
| $\tau$ | $=\text{sign}(p_w)\times\sin\gamma$ |

*Subscripts*

| | |
|---|---|
| $f$ | =final |
| $o$ | =initial |
| $s$ | =mean sea level |

## Introduction

FOR a maneuvering re-entry vehicle, the pursuit of maximum-terminal velocity in the atmosphere has the advantages of reducing time to satisfy end constraints and providing energy management for subsequent terminal maneuvers. One subtopic in this area is the plane change maneuver,[1] in which the flight heading is changed. The problem of plane change in the upper reaches of the atmosphere has been solved previously for the case of small vertical flight-path angle $\gamma$. This paper presents a solution for the case of large $\gamma$, enabling plane changes to occur at any altitude during descent, while maximizing terminal velocity. Previous work[2,3] on the plane change problem concentrates on orbital plane change, where the flight-path angle remains small to maintain energy. However, if it is desired to execute large altitude changes within the atmosphere, then more flexibility is needed to control the velocity orientation.

The purpose of this study is to devise approximate, analytical, optimal control rules that can be computed repetitively to provide real-time maximum-terminal-velocity steering. The solution is derived from an integrable system of equations in terms of $\gamma$. The system is obtained by first making approximations to the equations of motion consistent with the intended trajectories. The optimal control problem is then specified, and control laws are derived. The control computations are implemented in a sample-data guidance scheme, and the results are compared for usage in both an approximate physical model and a simulation of an actual vehicle.

## Equations of Motion

The equations of motion for a nonthrusting point mass traveling over a spherical, nonrotating Earth are

$$\dot{\theta}=\frac{V\cos\gamma\cos\chi}{(r_s+h)\cos\phi} \tag{1}$$

$$\dot{\phi}=\frac{V\cos\gamma\sin\chi}{r_s+h} \tag{2}$$

$$\dot{h}=V\sin\gamma \tag{3}$$

Received July 10, 1986; revision received Dec. 3, 1986. 

*Member, Technical Staff, Aerodynamics Department. Senior Member AIAA.
†M.J. Thompson Regents Professor, Department of Aerospace Engineering. Associate Fellow AIAA.

$$\dot{V}=-\frac{D}{m}-\frac{g_s r_s^2 \sin\gamma}{(r_s+h)^2} \tag{4}$$

$$\dot{\gamma}=\frac{L}{mV}-\left[\frac{g_s r_s^2}{V(r_s+h)^2}-\frac{V}{r_s+h}\right]\cos\gamma \tag{5}$$

$$\dot{\chi}=\frac{S}{mV\cos\gamma}-\frac{V\cos\gamma\cos\chi\tan\phi}{r_s+h} \tag{6}$$

where $(\dot{})=\mathrm{d}(\ )/\mathrm{d}t$. The coordinate system is given in Fig.1, where a local-horizon coordinate system ($xyz$) is shown with respect to an Earth-centered inertial system ($XYZ$). $\gamma$ is the flight-path angle measured positive outward and normal to the $xy$ plane and $\chi$ is the heading angle measured from the $x$ axis to the projection of the velocity vector in the $xy$ plane. The aerodynamic forces $L$, $S$, and $D$ are of the form

$$F=\rho V^2 S_R C_F/2 \tag{7}$$

where $C_F$ is the force coefficient. Although a bank-to-turn missile has been used in previous studies, a skid-to-turn missile is used here. Equations (1–6) form the *simulation* physical model in which the derived guidance laws are tested.

## Approximations to the Equations of Motion

As before,[2,3] aerodynamic forces are considered dominant, which eliminates the gravity component tangential to the velocity vector (i.e., $g|\sin\gamma| \ll D/m$). However, to expand the range of validity, Loh's approximation[4] is used to include inertial effects normal to velocity. Equation (5) can be rewritten as

$$\dot{\gamma}=\rho V\left(\frac{C_L S_R}{2m}+M\right) \tag{8}$$

where

$$M=\left[1-\frac{g_s r_s^2}{V^2(r_s+h)}\right]\frac{\cos\gamma}{\rho(r_s+h)} \tag{9}$$

which represents Loh's constant, a term that has been found to be insensitive to $\rho$ or $\gamma$ integration along re-entry trajectories.

For flight completely within the atmosphere, large cross-ranges are not covered, so that the term $V\cos\gamma\cos\chi$ $\tan\phi/(r_s+h)$ is negligible. Also $h \ll r_s$. These approximations reduce the equations of motion to the following:

$$\dot{h}=V\sin\gamma \tag{10}$$

$$\dot{V}=-\rho V^2 C_D S_R/2m \tag{11}$$

$$\dot{\gamma}=\rho V[C_L S_R/2m+M] \tag{12}$$

$$\dot{\chi}=\rho V C_s S_R/(2m\cos\gamma) \tag{13}$$

Since the angular position is not constrained, Eqs. (1) and (2) have been eliminated.

The vehicle is symmetric, and its drag polar is defined by a parabolic fit to wind-tunnel data for the actual vehicle,

$$C_D=C_{D_0}+\kappa C_S^2+\kappa C_L^2 \tag{14}$$

where $C_{D_0}$ and $\kappa$ are constants. If $C_S$ and $C_L$ are scaled by $C_L^*$, which corresponds to the maximum pitch $L/D$ ratio, then

$$C_D=C_{D_0}(1+\sigma^2+\lambda^2) \tag{15}$$

where $\sigma=C_S/C_L^*$, $\lambda=C_L/C_L^*$, and $C^*{}_L=(C_{D_0}/\kappa)^{1/2}$.

The atmospheric density is modeled with an exponential fit,

$$\rho=\rho_s e^{-h/\beta\alpha} \tag{16}$$

where $\rho_s=0.0023769$ slug/ft$^3$ and $\beta_\alpha=23{,}800$ ft. This model has been cited in Ref. 5. If Eq. (16) is differentiated, then it can be used in place of Eq. (10), and altitude can be eliminated from the equations of motion in favor of $\rho$.

These approximations result in the following *approximate* physical model:

$$\dot{\rho}=-\rho V\sin\gamma/\beta_\alpha \tag{17}$$

$$\dot{V}=-\rho V^2 S_R C_{D_0}(1+\sigma^2+\lambda^2)/2m \tag{18}$$

$$\dot{\gamma}=\rho V C_L^* S_R(\lambda+\bar{M})/2m \tag{19}$$

$$\dot{\chi}=\rho V C_L^* S_R\sigma/(2m\cos\gamma) \tag{20}$$

where

$$\bar{M}=2mM/C_L^* S_R \tag{21}$$

Since there is no boundary condition on time, it can be eliminated in favor of $\gamma$, which expedites a solution and is consistent with Loh's approximation.[4] Suitable nondimensional states chosen to replace $\rho$ and $V$ are

$$\omega=\frac{\rho}{2m/(\beta_\alpha S_R C_L^*)} \quad \text{and} \quad u=-\left(\frac{C_L^*}{C_{D_0}}\right)\ln V \tag{22}$$

Maximizing velocity now entails *minimizing* $u$. With these changes, the equations of motion used in the optimal control problem (OCP) are

$$\frac{\mathrm{d}\omega}{\mathrm{d}\gamma}=-\frac{\sin\gamma}{\lambda+\bar{M}} \tag{23}$$

$$\frac{\mathrm{d}u}{\mathrm{d}\gamma}=\frac{1+\sigma^2+\lambda^2}{\lambda+\bar{M}} \tag{24}$$

$$\frac{\mathrm{d}\chi}{\mathrm{d}\gamma}=\frac{\sigma/\cos\gamma}{\lambda+\bar{M}} \tag{25}$$

Depending on the end conditions of the trajectory, $\gamma$ may vary in a nonmonotonic fashion. In other words, an *inflection*

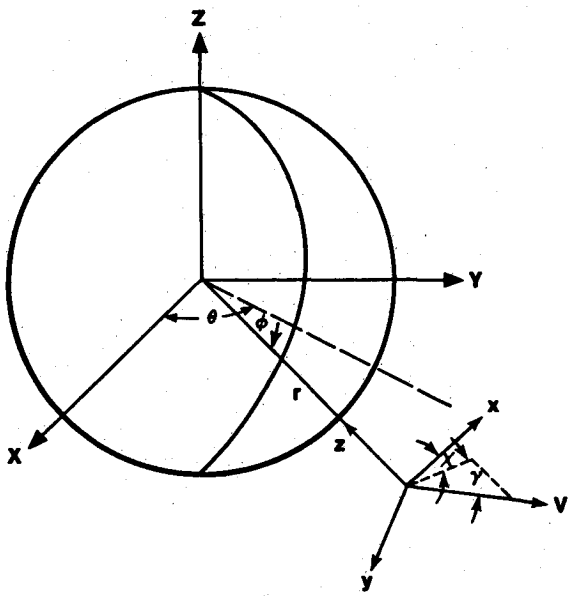


**Fig. 1 Coordinate systems.**

*point* $\gamma_i$, where $\lambda+\bar{M}=0$, may occur. This requires more involved integration techniques in solving the OCP.

## Optimal Control Problem

The goal is to maximize terminal velocity while constraining terminal altitude and heading for a descent trajectory. $\gamma_f$ may or may not be fixed. Initial conditions are given. The Hamiltonian and end function are

$$H=[-p_w\sin\gamma+p_u(1+\sigma^2+\lambda^2)+p_\chi\sigma/\cos\gamma]/(\lambda+\bar{M}) \quad (26)$$

$$G=u_f+\nu_1(w_f-w_{f_s})+\nu_2(\chi_f-\chi_{f_s}) \quad (27)$$

where $s$ implies a specified value.

Since $\gamma$ is the independent variable, no states appear in $H$ and, hence, the Lagrange multipliers are constants and equal to the following natural boundary values:

$$p_w=\nu_1, \qquad p_u=1, \qquad p_\chi=\nu_2 \quad (28)$$

The control equations $H_\sigma=H_\lambda=0$ give the following:

$$\sigma=-p_\chi/(2\cos\gamma) \quad (29)$$

$$(\lambda+\bar{M})^2=1+\bar{M}^2-p_w\sin\gamma-p_\chi^2/(4\cos^2\gamma) \quad (30)$$

The sign of $\lambda+\bar{M}$ is dictated by the desired variation of $\gamma$, (+) for increasing $\gamma$. The forms of $\sigma$ and $\lambda$ are nonlinear control laws and are usable once $p_w$ and $p_\chi$ are known.

If $\gamma_f$ is free, the boundary condition $G_{\gamma f}+H_f=0$ gives $\lambda_f=0$. If this is used in Eq. (30), the following cubic must be solved for $\gamma_f$:

$$\sin^3\gamma_f-\frac{1}{p_w}\sin^2\gamma_f-\sin\gamma_f+\frac{1-p_\chi^2/4}{p_w}=0 \quad (31)$$

At most, two of these roots are actual possibilities, and each must be investigated.

## Evaluation of the Lagrange Multipliers

By substituting the control forms in Eqs. (29) and (30) into the state equations (23) and (25), the following differential equations result:

$$\frac{dw}{d\gamma}=\frac{-\sin\gamma}{\pm[1+\bar{M}^2-p_w\sin\gamma-p_\chi^2/(4\cos^2\gamma)]^{1/2}} \quad (32)$$

$$\frac{d\chi}{d\gamma}=\frac{-p_\chi}{\pm 2\cos^2\gamma[1+\bar{M}^2-p_w\sin\gamma-p_\chi^2/(4\cos^2\gamma)]^{1/2}} \quad (33)$$

To implement the control laws, it is necessary to solve for $p_w$ and $p_\chi$ by first integrating these equations to compute final values of nondimensional density $w_f$ and heading $\chi_f$. With some manipulation, these equations can be rewritten in the following general differential form:

$$dx=\frac{v(\tau)d\tau}{\pm|p_w|^{1/2}(\tau^3+d\tau^2+e\tau+f)^{1/2}} \quad (34)$$

where $\tau=\text{sign}(p_w)\times\sin\gamma$,

$$v(\tau)=-\tau \qquad \text{for } x=w$$

$$=-0.5p_\chi/(1-\tau^2) \qquad \text{for } x=\chi \quad (35)$$

$$d=-\frac{1+\bar{M}^2}{|p_w|}, \qquad e=-1, \qquad f=\frac{1+\bar{M}^2-p_\chi^2/4}{|p_w|} \quad (36)$$

The radical in Eq. (34) has three roots $a$, $b$, and $c$ where $a$ is the largest. Only two of these roots qualify as inflection points (IP's). For plane changes where $\gamma$ remains small, only one IP is possible.[3] The radical above results in *elliptic integral* solutions, which are sectionalized according to the variation in $\tau$; that is, $\tau<c$, $c\le\tau<b$, $b\le\tau<a$, or $a\le\tau$. These solution forms are listed in the Appendix.

Since two IP's are possible, three kinds of trajectories satisfying the end conditions must be examined. These are a single arc of either increasing or decreasing $\gamma$, two arcs connected at an IP, or three arcs separated at two IP's. An examination of the Legendre and Weierstrass conditions has revealed that all possibilities are minimizing trajectories. Therefore, it has been necessary to test all trajectories that cannot be excluded on physical grounds. The general formulas of integration for trajectories containing 0,1, or 2 IP's are summarized by the following:

$$\int_{\tau_1}^{\tau_2}dx=\begin{cases}\pm[x(\tau_2)-x(\tau_1)]\\ \pm[x(\tau_2)+x(\tau_1)-2x(\tau_{i_1})]\\ \pm[x(\tau_2)-x(\tau_1)+2x(\tau_{i_1})-2x(\tau_{i_2})]\end{cases} \quad (37)$$

where each term in a formula is the result of single or combined elliptic integral solutions with a common *lower* limit (either $-\infty$, $c$, $b$, or $a$). The $\pm$sign indicates a final arc of either increasing (+) or decreasing (−) $\gamma$. A sample computation is also given in the Appendix.

Since $p_w$ and $p_\chi$ are embedded in elliptic integrals, a complete algebraic solution is not possible. A Newton scheme is used to isolate these multipliers from the solution of Eq. (34). To start, a trajectory or integration formula in Eq. (37) is assumed. Some information is gained for initial multiplier guesses from the small $\gamma$ solution by Hull.[3] With these initial values, the cubic in Eq. (34) can then be solved for the IP's and the one in Eq. (31), for $\gamma_f$, if this condition is free. The two forms of Eq. (34) can then be integrated according to the assumed formula to ensure that the specified final conditions are met for the guessed values of $p_w$ and $p_\chi$. If not, the multipliers are incremented until convergence is achieved. If the assumed trajectory is not realizable, the iterative solution technique causes the cubic roots to migrate rapidly toward known singularities in one or more of the elliptic integrals shown in Eqs. (A1–A11) in the Appendix.

Once $p_w$ and $p_\chi$ have been found, an approximate optimal trajectory and control histories can be computed for a single value of $\bar{M}$ from the current initial conditions to the specifed final conditions. In an actual sample-data guidance setting, the problem is resolved at each sample point along the trajectory, updating initial conditions and the approximate physical model via $\bar{M}$ with information received from onboard inertial measurement units.

## Results

The results compare four kinds of trajectory data. These are:

1) A single, approximate optimal trajectory computed from the solutions to Eqs. (23–25) for the case of $\bar{M}$ constant.

2) An approximate optimal trajectory, where the controls are repetitively computed based on updated initial conditions and an updated approximate physical model due to changing $\bar{M}$ at the sample points to reflect any variation in the combination of $\rho$, $\gamma$, and $V$.

3) A numerical control approximation for a modified-approximate physical model using the parameter optimization code, VFO2AD. In this model, $\bar{M}$ is allowed to vary continuously. The results of this *off-line* control solution technique are meant to verify those *on-line* in 2, assuming rapid updating in 2.

4) Finally, control computations as outlined in 2 but operating within the simulation physical model.

In the computations for 1 and 2, time has been eliminated from the OCP in favor of $\gamma$. However, for updating and comparison purposes, it is convenient to create a time/flight-path-

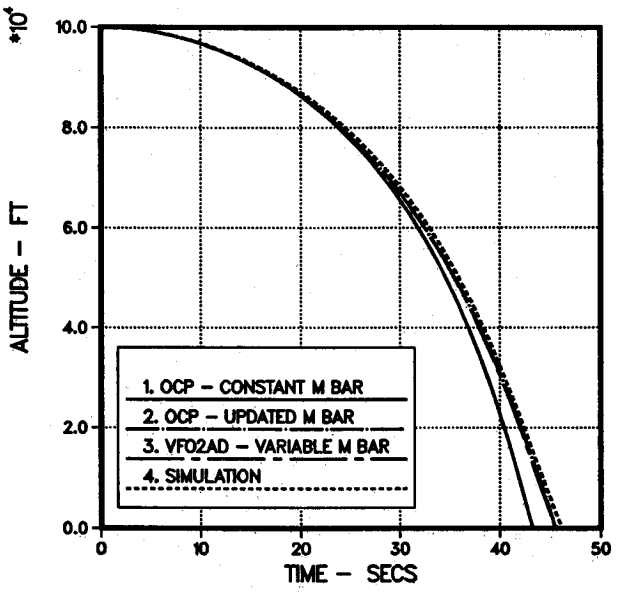


Fig. 2a Altitude vs time.

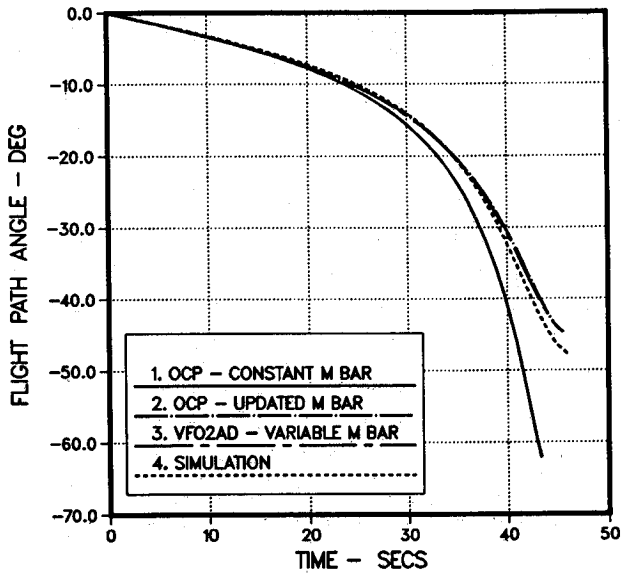


Fig. 2b Flight path angle vs time.

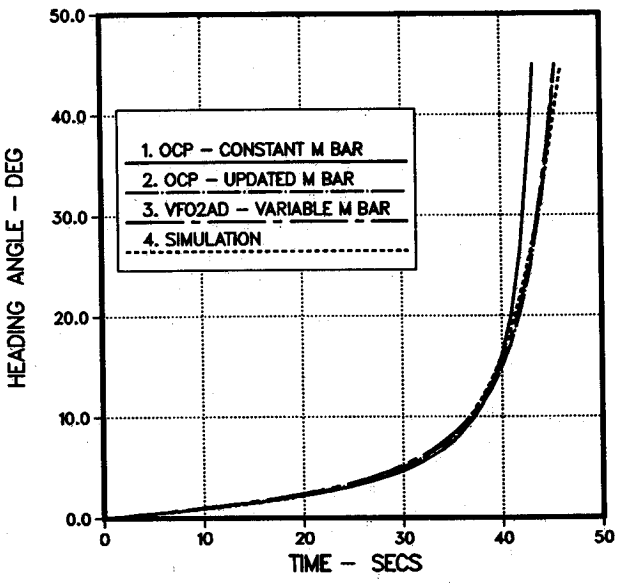


Fig. 2c Heading vs time.

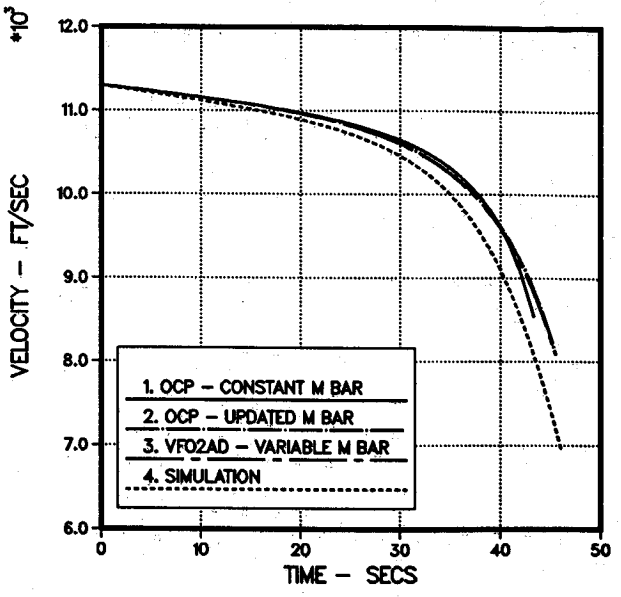


Fig. 2d Velocity vs time.

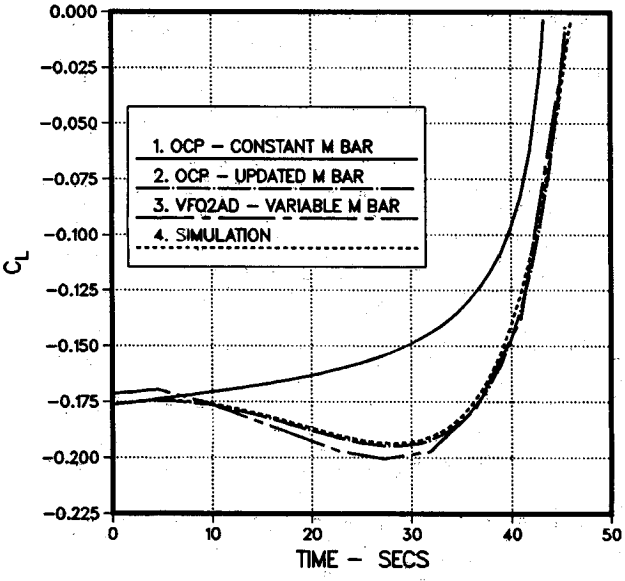


Fig. 2e Lift force coefficient vs time.

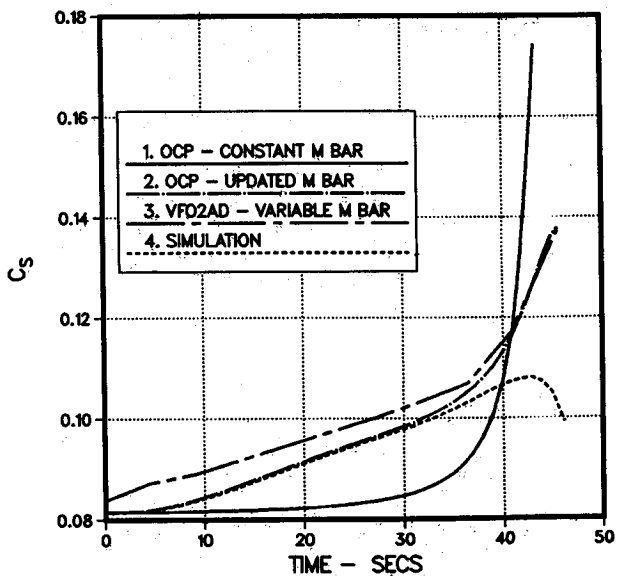


Fig. 2f Side force coefficient vs time.

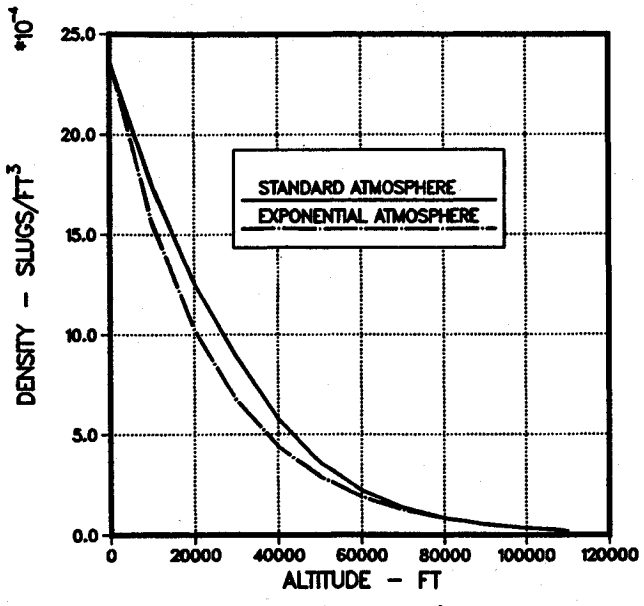


**Fig. 3 Atmosphere comparison.**

angle base for these computations, using the Euler form

$$\gamma(t_{k+1}) = \gamma(t_k + \Delta t) = \gamma(t_k) + \dot{\gamma}(t_k)\Delta t \qquad (38)$$

where $\dot{\gamma}$ is given in Eq. (19). This is necessary in 2 where $\bar{M}$ is updated every $\Delta t$ (0.1 s) to reflect the changes in $V$, $\gamma$, and $\rho$. The simulation (4) provides its own time base, using a fourth-order Runge-Kutta integrator on Eqs. (1-6). VFO2AD uses the method of Recursive Quadratic Programming developed by Powell.[6] The parameters are the force coefficients $C_L$ and $C_S$ at eleven points (*node* points) along the trajectory.[1] Linear interpolation is used to compute controls between nodes. Each parameter is perturbed, and trajectory-based numerical derivatives of the performance index $V_f$ and constraints $\rho_f$, $\chi_f$ are computed.

The standard atmosphere and a wind-tunnel-based aerodynamic package for a representative skid-to-turn vehicle are used in simulation. The controls are held fixed over the *sample* time (0.1 s).

Trajectory initial conditions include the following:

$$h_0 = 100{,}000 \text{ ft}, \qquad V_0 = 11{,}300 \text{ ft/s}$$

$$\gamma_0 = 0 \text{ deg}, \qquad \chi_0 = 0 \text{ deg}$$

Results are displayed in Figs. 2a-2f for the case of $h_f = 0$ ft, $\chi_f = 45$ deg, and $\gamma_f =$ free. (Note that M BAR $= \bar{M}$.) Altitude, flight-path, and heading histories (Figs. 2a-2c) agree for cases 2-4, in which $\bar{M}$ is variable. Variations vs the single constant-$\bar{M}$ trajectory stem from the fact that $\bar{M}$ is actually vanishing during descent.

Note that, in Fig. 2c, the majority of the heading change occurs in the final portion of flight. Since $\sigma = -p_x/2\cos\gamma$, the guidance logic is taking advantage of the steepest portion of the trajectory, which happens near the end, to apply the most turning. In descent, this is advantageous, because the density increases, allowing lower commanded $\sigma$'s for a desired heading rate. However, as a result of the late heading change, these maximum-terminal-velocity trajectories produce small cross-range changes.

The velocity histories (Fig. 2d) show a marked degradation of simulation results 4 vs the approximate optimals. This is due to the atmospheric mismatch between the standard and exponential model. As expected, agreement is quite good between computations 2 and 3.

**Table 1 Terminal velocities for $h_f = 0$ ft, $\chi_f = 45$ deg**

| $\gamma_f$ deg | 1 ft/s | 2 ft/s | 3 ft/s | 4 ft/s |
|---|---|---|---|---|
| 0 | 6609 | 7175 | 7142 | 5480 |
| −45 | 8371 | 8028 | 8081 | 6875 |
| −85 | 8273 | 7284 | 7250 | 6528 |
| Free | 8541 | 8084 | 8088 | 6953 |

The lift coefficient (Fig. 2e) shows that the vehicle guides in the vertical plane identically between computations 2 and 4. Computation 2 differs slightly from the VFO2AD results 3 for a negligible improvement in $V_f$.

The side force coefficient (Fig. 2f) is a more graphic illustration of atmospheric differences, where the simulation results show an initial increase followed by a decrease to satisfy $\chi_{f_s}$. Figure 3 shows the density variation between the atmospheric models. Note that the exponential can vary as much as 20% from the standard. Since the guidance model assumes a lower density in the 5-70-kft range, it tends initially to oversteer the vehicle in this region. It can be shown that a "floating" exponential fit of the atmosphere will alleviate this problem.

A summary of terminal velocities from the four computations is provided in Table 1 for a variety of $\gamma_f$.

The $\gamma_f$ -free trajectories produce the highest velocities as expected; however, the velocity for the free-$\gamma_f$ case approaches that of $\gamma_f = -45$ deg in 2, 3, and 4, as can be seen in the table. Computations 2 and 3 are extremely close, as predicted, and simulation results 4 are noticeably degraded due to the atmospheric differences depicted in Fig. 3. This degradation has been substantiated by VFO2AD solutions, using the simulation physical model. These numerical results show $V_f =$ 5620/($\gamma_f =$ )0 deg, 6930/−45, 6563/−85, and 6974/free.

## Conclusions

A guidance method has been presented to generate maximum-terminal-velocity trajectories for a descending turn to a fixed heading, altitude, and if desired, flight-path angle. The continuous optimal guidance in which the controls are repetitively computed based on updates at each sample point has been verified by a numerical optimization process. Guidance policies in simulation agree with those generated in an updated, approximate physical model, if the approximate atmosphere is reasonably close to the true.

## Appendix

Standard elliptic integrals[7,8] are used in evaluating the differential forms in Eq. (34). Depending on the variation in $\tau$, the integration of Eq. (34) can generate a variety of solutions as shown in Eq. (37). To conform to the standard integral forms, as well as facilitate computer coding, each term in Eq. (37) is evaluated with respect to a common lower limit. For example, in the formula

$$\int_{\tau_1}^{\tau_2} dx = \pm [x(\tau_2) - x(\tau_1)] \qquad (A1)$$

$x(\tau_2)$ and $x(\tau_1)$ are the results of integrations with respect to a lower limit, say, $c < \min(\tau_2, \tau_1)$, and upper limits $\tau_2$ and $\tau_1$, respectively. Since the span $c$-$\tau_2$ may contain roots of the radical in Eq. (34), more than one elliptic solution may be necessary to complete the spans. As adopted from Ref. 7, either $-\infty$ or one of the cubic roots $(c,b,a)$ is used as the lower limit. This procedure can just as readily be carried out for common fixed upper limits.

To make use of standard integrals, the differential for $\chi$ has been factored as follows:

$$d\chi = \frac{-0.5p_x}{(\pm |p_w|^{1/2})}\left[\frac{d\tau}{2(1+\tau)A} + \frac{d\tau}{2(1-\tau)A}\right] \qquad (A2)$$

where $A=(\tau^3+d\tau^2+e\tau+f)^{1/2}$. The $\pm$ grouped with $|p_w|^{1/2}$ denotes the direction of $\gamma$ change. Combined elliptic forms $X_\pm(\tau)$ are listed in this study to reflect the two terms inside the above brackets, where

$$\int_{\tau_1}^{\tau_2} d\chi=\int_{\tau_1}^{\tau_2}(dX_+ + dX_-)=[X_+(\tau_2)-X_+(\tau_1)] + [X_-(\tau_2)-X_-(\tau_1)] \quad \text{(A3)}$$

conforming to the integration formula in Eq. (39). The $X_\pm$ forms use additional $\pm$ signs for the respective $(1\pm\tau)$ factors in the denominators in Eq. (A2). Each of these forms is also computed with respect to the common lower limit.

The elliptic integrals for $w$ and $X_\pm$ are listed below for the various values of $\tau$.

$-\infty<\tau\le c$

$$w(\tau)-w(-\infty)=-\frac{n(a-c)}{\pm|p_w|^{1/2}}\left[F(\delta,j)-E(\delta,j)-\left[\frac{(c-\tau)(b-\tau)}{(a-c)(a-\tau)}\right]^{1/2}\right] \quad \text{(A4)}$$

$$X_\pm(\tau)-X_\pm(\infty)=\frac{np_\chi}{\pm 4|p_w|^{1/2}(1\pm a)}\left[\Pi\left(\delta,-\left[\frac{a\pm1}{a-c}\right],j\right)-F(\delta,j)\right] \quad \text{(A5)}$$

where

$$\delta=\sin^{-1}\left[\frac{a-c}{a-\tau}\right]^{1/2},\quad j=\left[\frac{a-b}{a-c}\right]^{1/2},\quad n=\frac{2}{\sqrt{a-c}}$$

$c<\tau\le b$

$$w(\tau)-w(c)=-\frac{1}{\pm|p_w|^{1/2}}[naF(\Delta,k)-2(a-c)E(\Delta,k)] \quad \text{(A6)}$$

$$X_\pm(\tau)-X_\pm(c)=-\frac{np_\chi}{\pm 4|p_w|^{1/2}(1\pm c)}\Pi\left[\Delta,\left(\frac{b-c}{c\pm1}\right),k\right] \quad \text{(A7)}$$

where

$$\Delta=\sin^{-1}\left[\frac{\tau-c}{b-c}\right]^{1/2},\quad k=\left[\frac{b-c}{a-c}\right]^{1/2}$$

$b<\tau\le a$

$$w(\tau)-w(b)=-\frac{n}{\pm|p_w|^{1/2}}[(b-c)\Pi(\mu,-l^2,l)+cF(\mu,l)] \quad \text{(A8)}$$

$$X\pm(\tau)-X_\pm(b)=-\frac{np_\chi}{\pm 4|p_w|^{1/2}(1\pm c)(b\pm1)}\left[(c-b)\Pi\left(\mu,-l^2\left[\frac{c\pm1}{b\pm1}\right],l\right)+(b\pm1)F(\mu,l)\right] \quad \text{(A9)}$$

where

$$\mu=\sin^{-1}\left[\frac{(a-c)(\tau-b)}{(a-b)(\tau-c)}\right]^{1/2},\quad l=\left[\frac{a-b}{a-c}\right]^{1/2}$$

$a\le\tau$

$$w(\tau)-w(a)=-\frac{n}{\pm|p_w|^{1/2}}[(a-b)\Pi(\omega,-1,m)+bF(\omega,m)] \quad \text{(A10)}$$

$$X_\pm(\tau)-X_\pm(a)=-\frac{\mp np_\chi}{\pm 4|p_w|^{1/2}(a\pm1)(b\pm1)}\times\left[(a-b)\Pi\left(\omega,-\left[\frac{b\pm1}{a\pm1}\right],m\right)-(a\pm1)F(\omega,m)\right] \quad \text{(A11)}$$

where

$$\omega=\sin^{-1}\left[\frac{\tau-a}{\tau-b}\right]^{1/2},\quad m=\left[\frac{b-c}{a-c}\right]^{1/2}$$

Approximations for $F$, $E$, and $\Pi$ are obained from IMSL[9] subroutines.

As an example computation, assume a maximum-terminal-velocity descent trajectory with positive heading change and a $\gamma_f$-free end condition. Typically for this trajectory, $0\ge\gamma_0=\gamma_1>\gamma_f=\gamma_2$, and the assumed $p_w$ and $p_\chi$ are both negative. This gives rise to $\tau_2>\tau_1$. In addition, let the $\gamma$-boundary conditions be related to the cubic roots by $a>b>\tau_2>c>\tau_1$. Therefore, the common lower limit for $\tau_1$, $\tau_2$ is $-\infty$.

To isolate the correct Lagrange multipliers, it is necessary to compare the computed density and heading changes with those specified. The dimensionless density-change computation for this example is given by

$$\int_{\gamma_1}^{\gamma_2} dw(\gamma)=\int_{\tau_1}^{\tau_2}\frac{-\tau dt}{-|p_w|^{1/2}A}$$

$$=\frac{1}{|p_w|^{1/2}}\left(\left[\int_c^{\tau_2}\frac{\tau d\tau}{A}+\int_{-\infty}^{c}\frac{\tau d\tau}{A}\right]-\int_{-\infty}^{\tau_1}\frac{\tau d\tau}{A}\right)$$

$$=([(w(\tau_2)-w(c))+(w(c)-w(-\infty))]-[w(\tau_1)-w(-\infty)])=w(\tau_2)-w(\tau_1),$$

or

$$=\frac{1}{|p_w|^{1/2}}\left[naF(\Delta(\tau_2),k)-2(a-c)E(\Delta(\tau_2),k)+n(a-c)\left(F(\delta(c),j)-E(\delta(c),j)-F(\delta(\tau_1),j)+E(\delta(\tau_1),j)+\left[\frac{(c-\tau_1)(b-\tau_1)}{(a-c)(a-\tau_1)}\right]^{1/2}\right)\right]$$

The heading-change computation is given by

$$\int_{\gamma_1}^{\tau_2} d\chi(\gamma)=\int_{\gamma_i}^{\gamma_2}\frac{-0.5p_\chi}{-|p_w|^{1/2}}\left[\frac{d\tau}{2(1+\tau)A}+\frac{d\tau}{2(1-\tau)A}\right]$$

$$=\int_{\tau_1}^{\tau_2}(dX_+ + dX_-)=\int_c^{\tau_2}(dX_+ + dX_-)$$

$$+\int_{-\infty}^{c}(dX_+ + dX_-)-\int_{-\infty}^{\tau_1}(dX_+ + dX_-)$$

$$=([X_+(\tau_2)-X_+(c)]+[X_-(\tau_2)-X_-(c)])$$

$$+([X_+(c)-X_+(-\infty)]$$

$$+[X_-(c)-X_-(-\infty)])-([X_+(\tau_1)-X_+(-\infty)]$$

$$+[X_-(\tau_1)-X_-(-\infty)])$$

$$=[X_+(\tau_2)-X_+(\tau_1)]+[X_-(\tau_2)-X_-(\tau_1)]$$

or

$$= \frac{np_\chi}{4\,|p_w|^{1/2}} \left( \frac{\Pi[\Delta(\tau_2),[(b-c)/(c+1)],k]}{1+c} \right.$$

$$+ \frac{\Pi[\Delta(\gamma),[(b-c)/(c-1)],k]}{1-c}$$

$$- \frac{\Pi[\delta(c),-[(a+1)/(a-c)],j]-F(\delta(c),j)}{1+a}$$

$$- \frac{\Pi[\delta(c),-[(a-1)/(a-c)],j]-F(\delta(c),j)}{1-a}$$

$$+ \frac{\Pi[\delta(\tau_1),-[(a+1)/(a-c)],j]-F(\delta(\tau_1),j)}{1+a}$$

$$\left. + \frac{\Pi[\delta(\tau_1),-[(a-1)/(a-c)],j]-F(\delta(\tau_1),j)}{1-a} \right)$$

These computed changes are compared with the desired ones in density and heading for the assumed values of $p_w$ and $p_\chi$. If the two differ by more than a specified tolerance, iteration continues. The possible solutions exhibit varying degrees of complexity depending on the boundary conditions, which dictate the positioning of the $\gamma$-boundary values with respect to the cubic roots.

## References


[1]Hull, E.G. and Speyer, J.L., "Optimal Re-entry and Plane Change Trajectories," *Journal of the Astronautical Sciences,* Vol. XXX, April-June 1982, pp. 117-130.

[2]Speyer, J.L. and Womble, M., "Approximate Optimal Atmospheric Entry Trajectories," *Journal of Spacecraft and Rockets,* Vol. 8, Dec. 1971, pp. 1120-1125.

[3]Hull, D.G., Giltner, J.M., Speyer, J.L., and Mapar, J., "Minimum Energy-Loss Guidance for Aero-Assisted Orbital Plane Change," *Journal of Guidance and Control,* Vol. 8, July-Aug. 1985, pp. 487-493.

[4]Loh, W.H.T., *Dynamics and Thermodynamics of Planetary Entry,* Prentice-Hall, Englewood Cliffs, NJ, 1963.

[5]Miele, A., *Flight Mechanics, Vol. 1: Theory of Flight Paths,* Addison-Wesley, Reading, MA, 1962.

[6]Powell, M.J.D., "A Fast Algorithm for Nonlinearly Constrained Optimization Calculations," *Proceedings of the Biennial Conference on Numerical Analysis, 28 June-July 1977,* edited by G.A. Watson, Springer-Verlag, Berlin, Germany, 1978, pp. 144-157.

[7]Byrd, P.F. and Friedman, M.D., *Handbook of Elliptic Integrals for Engineers and Scientists,* 2nd ed., Springer-Verlag, Berlin, Germany, 1971.

[8]Gradshteyn, I.S. and Ryzhik, I.M., *Tables of Integrals, Series, and Products—Corrected and Enlarged Edition,* Academic Press, Orlando, FL, 1980.

[9]*IMSL Library,* IMSL, Houston, TX, June 1982.